An experimental investigation of convection heat transfer during filling of a composite-fibre pressure vessel at low Reynolds number

An experimental investigation of convection heat transfer during filling of a composite-fibre pressure vessel at low Reynolds number

Melissa Heath

School of Engineering, Griffith University

Gold Coast Campus, Qld, 4222, Australia

E-mail: melissa.heath@griffithuni.edu.au

Peter Lloyd Woodfield, (corresponding author)

School of Engineering, Griffith University

Gold Coast Campus, Qld, 4222, Australia

E-mail: p.woodfield@griffith.edu.au

TEL: +61-7-5552-7501

Wayne Hall

School of Engineering, Griffith University

Gold Coast Campus, Qld, 4222, Australia

E-mail: w.hall@griffith.edu.au

TEL: +61-7-5552-9278

Masanori Monde

Department of Mechanical Engineering, Saga University

1 Honjo-machi, Saga, 840-8502, Japan

E-mail: monde@me.saga-u.ac.jp

Abstract

The heat transfer process during filling of an evacuated vessel at low Reynolds number was investigated experimentally using air as the flow medium. The data was analysed using a thermodynamic model similar to one currently in use for the design of systems using commercial carbon fibre reinforced plastic vessels for storage of compressed hydrogen gas. Model assumptions included perfectly-stirred conditions within the vessel, one-dimensional unsteady heat conduction through the composite vessel wall, ideal gas and frictional adiabatic flow conditions through the inlet tube. A transition phenomenon from laminar to turbulent flow was observed by decreasing the inlet diameter while maintaining a similar mass flow rate. Based on the measurements, a new empirical correlation for the Nusselt number under low Reynolds number flow conditions is proposed.

Keywords: convection heat transfer correlation; composite pressure vessel

Nomenclature

a = thermal diffusivity

A = inside area of vessel

c = sound speed of air

c_s = specific heat for solid

C_p = constant pressure specific heat of gas

d = internal diameter of supply pipe

D = internal diameter of experimental vessel

g = acceleration due to gravity

H = internal height of vessel

h_a = specific internal enthalpy of supply

h_f = head loss due to friction in supply pipe

L = length of supply pipe

m = mass of gas in vessel

M = Mach number

$\dot{M}$ = mass flow rate

Nu = Nusselt number

P = Pressure in vessel

r = radial position in the wall

Ra = Rayleigh number

Re = Reynolds Number

R_{air} = ideal gas specific to air

R_{cyl} = internal radius of cylinder

R_{in} = inner radius

R_{out} = outer radius

t = time

t_w = thickness of vessel wall

T_a = supply temperature of gas

T_e = environment temperature

T_g = gas temperature

T_o = initial temperature of gas

T_s= temperature of solid

T_w = inside temperature of wall

u = specific internal energy

v = velocity in supply pipe

V = internal volume of vessel

V_f = Volume fibre fraction

Greek

α_e = convection heat transfer coefficient from outside wall to environment

α_h = convection heat transfer coefficient from gas to the wall

β = volumetric thermal expansion coefficient

λ = thermal conductivity

ν = Poisson's ratio

μ = dynamic viscosity

ρ = density

τ = Fourier number = atR_{cyl}^{-2}

1. Introduction

This study is part of a larger investigation to explore heat transfer processes that occur during pressurizing and depressurizing of gas containment vessels. The theme has particular importance for carbon fibre reinforce plastic vessels used in fuel cell vehicles which have problems with overheating during the semi-adiabatic compression process during filling [1-8]. Other applications include accidental depressurization where the concern may be excessive internal cooling of a metal container [9] and predictions of gas leakage rates from vessels [10]. For mobile applications, vessel sizes typically range from a few litres suitable for hydrogen powered scooters or bicycles [11] to banks of 200 litre vessels used in fuel cell buses [12]. For applications which require very small vessels, metal hydride hydrogen storage has been given relatively more attention than compressed storage in the literature based on the perception that it is safer [13]. Compressed gas storage is still the most popular choice for commercial hydrogen fuel cell cars.

When filling pressure vessels with compressed gas, flow work is done in the container which causes heating. In the case of carbon fibre reinforced plastic (CFRP) vessels it becomes particularly important to be able to predict the temperature rise since the material is sensitive to high temperatures. A number of studies have considered computational fluid dynamics (CFD) modelling [3-6] and experimentation where the temperature during filling was monitored [7, 8]. Somewhat surprisingly, most research has focused on the temperature of the gas rather than the temperature distribution in the vessel wall and there appears to be a lack of fundamental data describing the heat transfer process. Very little attention has been given to heat transfer in this flow situation at low Reynolds number.

Recently, Winters et al. [14] experimentally and numerically investigated heat transfer during depressurization of a spherical vessel. They found good agreement between their results and an analytical model by Paolucci [15] during the early stages of gas expansion followed by a period of time where natural convection heat transfer dominated. Charton et al. [9] considered the flow of gas into an evacuated vessel connected to a pressurized vessel via a thin tube. Their experimental data was in reasonable agreement with predictions from a thermodynamic model which utilized a natural convection heat transfer correlation for both the supply vessel and the receiver. In their model, the correlation used for the Nusselt number was of the form $Nu = CRa^n$ where C is a constant and n is approximately 0.25 for laminar natural convection and 1/3 for turbulent natural convection [16, 17]. Woodfield et al. [18], in their study on depressurizing and pressurizing of gas storage vessels, found that heat transfer during filling of the vessel was better described using a mixed convection heat transfer correlation involving both the inlet tube Reynolds number and the Rayleigh number. Their correlations captured most of their own data well but under-predicted the heat transfer during the very early stages of depressurizing of the vessel. In commercial applications it is common to assume that the heat transfer coefficient has a constant value for entire filling process [2].

Because of safety issues in the use of high-pressure hydrogen gas, we are seeking to develop low-pressure physical models suitable for exploring the details of the science of heat transfer within a confined pressurizing or depressurizing flow field. By developing such models, detailed experimental investigations can be carried out both safely and cost effectively. In this study we are using a small vessel that is initially evacuated and then filled with ambient air whilst simultaneously monitoring the temperatures in the flow field to elucidate the heat transfer process. This approach has an added merit that the ambient supply can be modelled accurately as an infinite source with a constant specific enthalpy. The conditions considered correspond to the low Reynolds number regime for this class of flow problems.

2. Design and construction of experimental vessel

Composite pressure vessels are often constructed using a filament winding technique (e.g. [19]). For our purpose, however, it is desirable to have the option of embedding thermocouples in the wall itself in between layers of fibre. To give us this flexibility we opted for a vacuum bag resin infusion technique, which we have available in our laboratory, for constructing the composite vessel. The experimental vessel was designed to support an internal vacuum, or 1 atmosphere of external pressure. The vessel was cylindrical in shape and had an internal radius of 0.035 m and an internal height of 0.180 m.

The composite vessel was constructed in four pieces – two cylindrical halves and two flat ends. Fig. 1 gives an illustration of the vessel with one of the cylindrical halves removed for clarity. This design was chosen to enable accurate positioning of the thermocouple junctions for measuring the gas temperature. Unidirectional carbon fibre with an area density of 200 g/m^2 was used in the construction. A mould was prepared from a half cylinder of mild steel, which had been machined to an external diameter of 70 mm. This was glued to a flat aluminium plate using a 2 part epoxy adhesive. The entire mould was coated with epoxy and cured for 4 hours at 80 °C, before sanding to achieve a smooth finish. Endplates were cut from Perspex and clamped in place during construction. After laying up two layers of fabric, thermocouples were embedded into the wall. The constructed vessel wall had a total of twelve layers of fibre and a final thickness of 4.0 mm.

3. Experimental setup

Fig. 2 shows a schematic of the experimental setup. To monitor temperature history and determine heat transfer during the experiment, fourteen thermocouples were used with four inside the vessel wall, eight inside the gas (in the positions shown in Fig. 1), one measuring the ambient temperature and one measuring the temperature of the air inside the supply tube just before valve 1. The

thermocouples in the wall were at the same vertical positions as those in the gas shown in Fig. 1. All thermocouples were connected to a multi-channel digital multimeter which itself was connected to a personal computer via a GPIB link. Flow into the vessel was controlled using a long supply tube (30 m in length) with a small diameter (1.59 mm internal diameter) (see Fig. 2). The internal diameter of the tube was measured gravimetrically by filling a long section of the tube with water which was subsequently measured and weighed.

The pipe connections were push-fit union type joints suitable for air and gas at low pressure. The vacuum pressure gauge shown in Fig. 2 was used to measure the initial and final pressures in the cylinder. The known geometry of the supply tube allowed for a well controlled and predictable flow of air into the vessel. The thermal camera was used to confirm the uniformity of the initial internal wall temperature distribution. As illustrated in Figs 1 and 2, air enters the cylinder through the bottom plate and the cylinder is orientated such that its axis is vertical during the experiment. The diameter of the air inlet to the cylinder can be changed by inserting tubes with different inside diameters into the inlet port shown in the bottom of the vessel in Fig. 1. For this study, two different inside diameters were considered, 1.59 mm and 5.25 mm.

The experiment itself was conducted as follows: With valve 1 closed and valve 2 open, air inside the vessel was evacuated using the vacuum pump until the pressure reached 2.5 kPa (abs). Time (several minutes) was then allowed for the temperature of the vessel to return to equilibrium. The temperature uniformity was verified with the thermal camera. Valve 2 was then closed and thermocouple measurements were initiated before opening valve 1 to allow the vessel to fill. Data was recorded for about 200 seconds with a sampling rate of about 0.1 second per reading (i.e. about 1.5 seconds to sweep across all temperature sensors).

4. Theoretical model

A theoretical model based on a study by Monde et al. [2] was developed to simulate the filling process. From the energy balance for the entire vessel, the inflow of energy (the mass flow rate multiplied by the specific enthalpy) minus the outflow of energy (i.e. heat transfer through wall) is equal to the rate of change of internal energy in vessel. This is given by:

$$\dot{M}h_a - \alpha_h A\left(T_g - T_w\right) = \frac{d}{dt}\left(mu\left(P, T_g\right)\right) \tag{1}$$

The initial condition for Eq. (1) is that the temperature of the gas at time = 0 is equal to T_0 as shown in:

$$T_g\,|_{t=0} = T_0 \tag{2}$$

Density is found using the ideal gas equation, as a low pressure situation is assumed.

$$\rho\left(P, T_g\right) = \frac{P}{R_{air} T_g} \tag{3}$$

Unsteady 1D heat conduction through the wall is given by:

$$\rho_s c_s \frac{\partial T_s}{\partial t} = \frac{1}{r} \frac{\partial}{\partial r}\left(r \lambda_s \frac{\partial T_s}{\partial r} \right) \tag{4}$$

The boundary conditions inside and outside of the wall are given by:

$$-\lambda_s \frac{\partial T_s}{\partial r}\,|_{r=R_{in}} = \alpha_h \left(T_g - T_s\,|_{r=R_{in}} \right) \tag{5}$$

$$-\lambda_s \frac{\partial T_s}{\partial r}\,|_{r=R_{out}} = \alpha_e \left(T_s\,|_{r=R_{out}} - T_e \right) \tag{6}$$

The mass flow rate into the vessel is calculated using a frictional adiabatic flow model with known geometry of the supply tube and the difference in pressure between the start and end of the tube. From continuity and the ideal gas equation, the rate of change of pressure can be tied to the mass flow rate:

$$\dot{M} = \frac{dm}{dt} = \frac{d}{dt}\left(\rho V\right) = \frac{d}{dt}\left(\frac{PV}{R_{air} T_g} \right) \tag{7}$$

Applying the continuity equation, the momentum equation and the first law of thermodynamics to the supply tube gives Eq. (8) and (9) for an ideal gas (e.g. [20]) under frictional adiabatic flow conditions.

$$\frac{P}{P^*} = \frac{1}{M}\left[\frac{\left(k+1\right)/2}{1 + M^2\left(k-1\right)/2} \right]^{\frac{1}{2}} \tag{8}$$

$$\frac{1 - M^2}{kM^2} + \frac{k+1}{2k} \ln\left[\frac{\left(k+1\right) M^2}{2\left(1 + M^2\left(k-1\right)/2\right)} \right] = \frac{\bar{f} L_{\max}}{d} \tag{9}$$

In Eq. (9), $L_{\max}$ is the theoretical length of the pipe corresponding to the position where the Mach number becomes unity. In Eq. (8), P is the pressure at the position where the Mach number M is specified and P^* is the pressure at the hypothetical position corresponding to a Mach number of unity.

The heat transfer coefficient α_h inside the vessel is specified using:

$$\alpha_h = \frac{Nu\lambda}{H} \tag{10}$$

Where the Nusselt number *Nu* [18], Reynolds number and Rayleigh number are:

$$Nu = 0.56\,\mathrm{Re}^{0.67} + 0.104\,Ra^{0.352} \tag{11}$$

$$\mathrm{Re} = \frac{\rho v d}{\mu} = \frac{4\dot{M}}{\mu\pi d} \tag{12}$$

$$Ra = \frac{g\beta\left(T_g - T_w\right)C_p\rho^2 H^3}{\mu\lambda} \tag{13}$$

A key role of this study is to test Eq. (11) in the context of a set of flow conditions that are different to those under which the equation was developed.

5. Numerical implementation of model

In order to solve the energy equation for the temperature of the gas numerically, Eq. (1) is rewritten in the form:

$$V\frac{d}{dt}\rho\left(P,T_g\right)h_a - \alpha_h A\left(T_g - T_w\right) = V\frac{d}{dt}\left(\rho\left(P,T_g\right)u\left(P,T_g\right)\right) \tag{14}$$

This is then numerically approximated over a small time step Δt.

$$h_a V\left(\rho\left(P,T_g\right) - \rho'\right) - \alpha_h A\left(T_g - T_w\right)\Delta t - V\left(\rho\left(P,T_g\right)u\left(P,T_g\right) - \rho' u'\right) = 0 \tag{15}$$

In Eq. (15) ρ' and u' are the density and specific internal energy from the last time step. T_w is obtained by solving for the temperature distribution through the wall using Eqs. (4) to (6) which are approximated using the finite volume method [21]. Equations (4), (8), (9) and (15) are solved simultaneously in a computer program written by the first author.

6. Experimental results

6.1 Uncertainty analysis

An uncertainty analysis on a 95% confidence interval (i.e. k=2) was carried out using the sequential perturbation method described by Moffat [22]. The relative uncertainty in the measured temperatures

was estimated at ± 0.2 K over the present temperature range based on a comparison with a traceable platinum resistance thermometer which was calibrated according to ITS90. The uncertainty in the initial pressure measurement was ± 0.3 kPa and for the diameter of the supply tube it was estimated at 1%. Propagation of uncertainties yielded different values for the uncertainties in the heat transfer coefficients at different times during filling of the vessel. Heat transfer coefficient data with calculated uncertainties greater than 30% were generally omitted from the analysis.

6.2 Temperature measurements

Fig. 3 shows examples of the temperatures measured as the vessel filled for two different inlet diameters, 1.59 mm and 5.25 mm. In both cases the same supply tube was used (30 m long, 1.59 mm ID) so that the mass flow rate in both cases was similar. Fig. 1 shows the positions of the thermocouples listed in Fig. 3. The solid lines in Fig. 3 show the temperatures near the centre of the vessel and the dashed lines the temperatures offset from the centre. For Fig. 3(a), the temperature histories for the gas have three distinct features – a sharp initial rise, a period where the temperature is high and fluctuates rapidly and a final period where the temperature falls smoothly as filling is completed and the gas cools. In Fig. 3(a), the initial period where each of the gas temperatures rose rapidly occurred over the first 20 s. This was followed by a turbulent period which is evident in the fluctuations of the thermocouple readings. The turbulent period was the longest at the top of the vessel as is apparent from thermocouples G7 and G8. After the turbulent period, the temperatures began to fall smoothly as natural convection dominated. This interpretation is also consistent with the stratified temperature distribution with higher temperatures at the top of the vessel as is clear from Fig. 3(a) after time = 100 s. Based on the calculated flow rate using the frictional adiabatic model, at time = 100 s, the mass flow rate had dropped to about 3% of its initial rate which is also consistent with the changeover from forced to natural convection heat transfer. The behaviour shown in Fig. 3(b) is quite different to that shown in Fig. 3(a). The turbulent period where the gas temperatures are nearly uniform is absent. For the entire filling period, the thermal field is stratified and the maximum gas temperatures are significantly higher in Fig. 3(b) than in Fig. 3(a). It appears that the flow field is laminar in Fig. 3(b) as a result of the reduced jet Reynolds number. Increasing the jet diameter for the same mass flow rate has the effect of reducing the Reynolds number as is clear from Eq. (12).

The supply temperature was approximately 0.5°C cooler than the initial temperature within the wall and gas of the vessel for both of the runs in Fig. 3. This temperature difference is likely due to the fact that the supply tube (and its corresponding thermocouple) was located on the ground about 0.7 m below the vessel. The initial drop in the inlet temperature (about 0.4 °C during the first few seconds) is consistent with the frictional adiabatic model for the supply tube. A temperature drop of about 0.2 °C could be explained through the Joule-Thompson effect but this was not included in the model

which assumed ideal gas enthalpies. In the wall of the vessel for both of the runs shown in Fig. 3, the temperature rose 0.2 °C at the bottom and a maximum of 0.4 °C at the top of the vessel. All of the wall temperatures were almost constant from 50 s to 200 s.

6.3 Heat transfer

The temperature rise within the vessel is governed by the heat transfer coefficient α_h, and heat conduction into the vessel wall. Fig. 4 gives the overall heat transfer coefficient as a function of time for eight trial runs where the heat transfer coefficient is determined using direct measurements from the experiment. The heat transfer coefficient from the gas to the wall can be found by rearranging Eq. (14) for α_h, as in Eq. (16).

$$\alpha_h = \frac{\left(V \frac{d\rho}{dt} h_a - V \frac{d}{dt}(\rho u) \right)}{A(T_g - T_w)} \tag{16}$$

Equation (16) is basically the heat balance for the gas side of the experiment and as such the measurements of α_h are not influenced directly by the properties of the vessel wall since T_w is measured. For the experiment, A and V are known from the geometry of the vessel, the temperature of the gas T_g and temperature of the wall T_w are directly measured and the enthalpy h_a is calculated based on the temperature measured in the supply line near the inlet to the vessel. The density ρ and specific internal energy u are functions of both pressure and temperature. As only atmospheric pressure and the initial and final pressure in the vessel were recorded, this information was reconstructed through the use of the model for frictional adiabatic flow through the supply tube for the initial pressure and vessel geometry using the recorded gas temperature and pipe dimensions. It is worth mentioning that isothermal and incompressible flow models were also considered to determine the flow rate through the pipe and the results were very similar because of the low Mach number. Uncertainty in the supply tube diameter was an important factor in determining the overall uncertainty for the measurements.

The results given in Fig. 4 show two distinct groups, one turbulent and the other laminar. These correspond to the two cases shown in Fig. 3. One exception is trial 1 for an inlet diameter of 1.59 mm shown in Fig. 4. This particular case shows a transitional behaviour between turbulent and laminar flow. As time progresses all of the curves merge together as natural convection becomes dominant and the inlet flow conditions are no longer important.

6.4 Dimensionless groups

In order to facilitate comparison of the present results with the literature, appropriate dimensionless groups were calculated. Fig. 5 shows the evolution of the Reynolds Number (*Re*), Rayleigh Number (*Ra*) and Nusselt number (*Nu*) during filling of the vessel for the case of an inlet diameter of 1.59 mm.

The Reynolds numbers lower than 2000 show that the flow in the inlet pipe was laminar. As mentioned earlier, the flow inside the vessel however was probably initially turbulent based on the temperature fluctuations observed in Fig. 3(a). This shows that a laminar flow model is suitable for the pipe but a turbulence model may be required for computational fluid dynamics simulations of the flow field in the vessel even at the present low-Reynolds number conditions. The falling Reynolds number indicates that forced convection heat transfer will decrease as the vessel fills. On the other hand, the Rayleigh number has a peak at around 50 s indicating that the driving forces for natural convection become more important as time progresses and then eventually decrease as the filling is completed.

The measured Reynolds numbers and Rayleigh numbers individually fall within the range specified by Woodfield et al [18] from time 20 s to 60 s. However, combining the two using Eq. (11) yields Nusselt numbers that are mostly smaller than all of data reported by Woodfield et al [18]. Moreover, the correlation given by Eq. (11) was developed using a single vessel with dimensionless geometry ratios $d/D = 0.14$ and $H/D = 2.8$ whereas in the present experiment $d/D = 0.021$ or 0.07 and $H/D = 2.6$. Therefore it is clear that the present study corresponds to a region of data not previously investigated by the authors. Fig. 5 also gives a comparison between the measured Nusselt number and that calculated using Eq. (11). There are some notable differences. Apart from the first 10 seconds, the Nusselt number is over-predicted by the correlation. Also the shape of the predicted curve is notably different to the measurements during the early stages of filling. This highlights a weakness in either the model or in the heat transfer coefficient correlation.

Fig. 6(a) shows the measured Nusselt numbers against predictions using Eq. (11) for the eight experimental runs shown previously in Fig. 4. For the purpose of comparison, data from Ref. [18] are also included in the figure. It is clear from this figure that the present data correspond to a lower region of Nusselt number and that in spite of being an extrapolation, Eq. (11) generally gives the correct order of magnitude for Nu. The effect of changing the value of d/D however, appears to be exaggerated by the correlation. This is clear from a comparison of the differences between the triangle and square symbols in Fig. 6(a). As a percentage of the magnitude of the heat transfer coefficient, these differences appear to be relatively larger in Fig. 6(a) than in Fig. 4 comparing the laminar and turbulent flow regimes.

Equation (11) does not consider the ratio d/D or dimensionless time. Because of the low pressure, the thermal diffusivity of the air in the present experiment is very high. As a result, Fourier numbers are significantly higher than those of high-pressure gas experiments. Therefore, transient heat conduction may be an important mechanism for heat transfer in the present data. With this in mind, several attempts were made to modify the correlation using d/D and the Fourier number τ based on the radius of the cylinder to better capture the trends in the data. Only a marginal improvement could be made

without considering dimensionless time (τ). The following equation improves the correlation of the present data considerably.

$$Nu = 0.51\left(\tau^2 - 1.05\tau + 0.38\right)^{-1}\left(d/D\right)^{0.45}\,\mathrm{Re}^{0.67} + 0.104Ra^{0.352} \qquad (17)$$

Equation (17) is basically a modification of Eq. (11) in that the coefficient of the Reynolds number term is replaced by a function involving the dimensionless diameter and the Fourier number. Fig. 6(b) compares Eq. (17) with the measured Nusselt numbers. The data from Ref. [18] are also included in the figure. The improvement to correlating the present data leads to a slightly poorer correlation of the data by Woodfield et al. [18] in the vicinity of Nu = 100. Equation (17) is most suitable for τ< 1.5, for 0.021 < d/D < 0.14 and for Nu < 100.

7. Conclusions

The following may be concluded from this study:

1. For low Reynolds number flow conditions, a switch from a laminar to a turbulent flow regime was observed as a result of reducing the inlet diameter to the vessel while maintaining a similar filling rate.
2. The thermal field for laminar flow conditions was stratified with a considerably higher peak gas temperature (at the top of the vessel) than what was observed under turbulent flow conditions.
3. The present experimental data was used to expand and modify the heat transfer correlation previously developed by two of the authors [18] for filling pressure vessels to capture a wider range of dimensionless groups than is presently available in the literature.
4. Both forced and natural convection were present in the experiment and consequently the flow regime inside the vessel is best described as mixed convection.

References

[1] S. Maus, J. Hapke, C. N. Ranong, E. Wuchner, G. Friedlmeir, D. Wenger, Filling procedure for vehicles with compressed hydrogen tanks, Int. J. Hydrogen Energy 33 (2008) 2513-2519.

[2] M. Monde, P. L. Woodfield, T. Takano, M. Kosaka, Estimation of temperature change in practical hydrogen pressure tanks being filled at high pressures of 35 and 70 MPa, Int. J. Hydrogen Energy 37 (2012) 5723-5734.

[3] C. J. B. Dicken, W. Merida Modelling the transient temperature distribution within a hydrogen cylinder during refuelling, J. Numer. Heat Transfer Part A 53 (2008) 1-24.

[4] A. Suryan, H. D. Kim, T. Setoguchi, Three dimensional numerical computations on the fast filling of a hydrogen tank under different conditions, Int. J. Hydrogen Energy 37 (2012) 7600-7611.

[5] Y. Zhao, G. Liu, Y. Liu, J. Zheng, Y. Chen, L. Zhao, J. Guo, Y. He, Numerical study on fast filling of 70 MPa type III cylinder for hydrogen vehicle, Int. J. Hydrogen Energy 37 (2012) 17517-17522.

[6] M. Heitsch, D. Baraldi, P. Moretto, Numerical Investigations on the fast filling of hydrogen tanks, Int. J. Hydrogen Energy 36 (2011) 2606-2612.

[7] C. J. B. Dicken, W. Merida, Measured effects of filling time and initial mass on the temperature distribution within a hydrogen cylinder during refuelling. J Power Sources 165 (2007) 324-36.

[8] P. L. Woodfield, M. Monde, Y. Mitsutake, Heat transfer characteristics for practical hydrogen pressure vessels being filled at high pressure, J. Thermal Sci. Tech. 2 (2008) 241-253.

[9] S. Charton, V. Blet, J. P. Corriou, A simplified model for real gas expansion between two reservoirs connected by a thin tube, Chem. Eng. Sci. 51 (1996) 295-308.

[10] J. Xiao, J. R. Travis, W. Breitung, Hydrogen release from a high pressure gaseous hydrogen reservoir in case of a small leak, Int. J. Hydrogen Energy 36 (2011) 2545-2554.

[11] L. Cardinali, S. Santomassimo, M. Stefanoni, Design and realization of a 300 W fuel cell generator on an electric bicycle, J. Power Sources 106 (2002) 384-387.

[12] K. Haraldsson, A. Folkesson, P. Alvfors, Fuel cell busses in the Stockholm CUTE project – First experiences from a climate perspective, J. Power Sources 145 (2005) 620-631.

[13] J. J. Hwang, Review on development and demonstration of hydrogen fuel cell scooters, Renewable Sustainable Energy Reviews 16 (2012) 3803-3815.

[14] W.S. Winters, G.H. Evans, S.F. Rice, R. Greif, An experimental and theoretical study of heat and mass transfer during the venting of gas from pressure vessels, Int. J. Heat Mass Transfer 55 (2012) 8-18.

[15] S. Paolucci, Heat transfer during the early expansion of gas in pressurized vessels, Int. J. Heat Mass Transfer 28 (1985) 1525-1537.

[16] D. E. Daney, Turbulent natural convection of liquid deuterium, hydrogen and nitrogen within enclosed vessels, Int. J. Heat Mass Transfer 19 (1976) 431-441.

[17] L. B. Evans, N. E. Stefany, An experimental study of transient heat transfer to liquids in cylindrical enclosures, Chemical Engineering Progress Symposium Series, American Institute of Chemical Engineers 62 (1966) 209-215.

[18] P. L. Woodfield, M. Monde, Y. Mitsutake, Measurement of averaged heat transfer coefficients in high-pressure vessel during charging with hydrogen, nitrogen or argon gas, J. Thermal Sci. Tech. 2 (2007) 180-191.

[19] F. C. Shen, Filament wound structure technology overview, Mater. Chem. Phys. 42 (1995) 96-100.

[20] R. Fox, A. McDonald, Introduction to Fluid Mechanics, John Wiley & Sons, New York, 1992.

[21] T. V. Patankar, K. C. Karki, K. M. Kelkar, in 'Handbook of Fluid Dynamics', ed. by R. W. Johnson, CRC Press, Boca Raton USA, 1998.

[22] R. J. Moffat, Describing the uncertainties in experimental results, Exper. Therm. Fluid Sci. 1 (1988) 3-17.

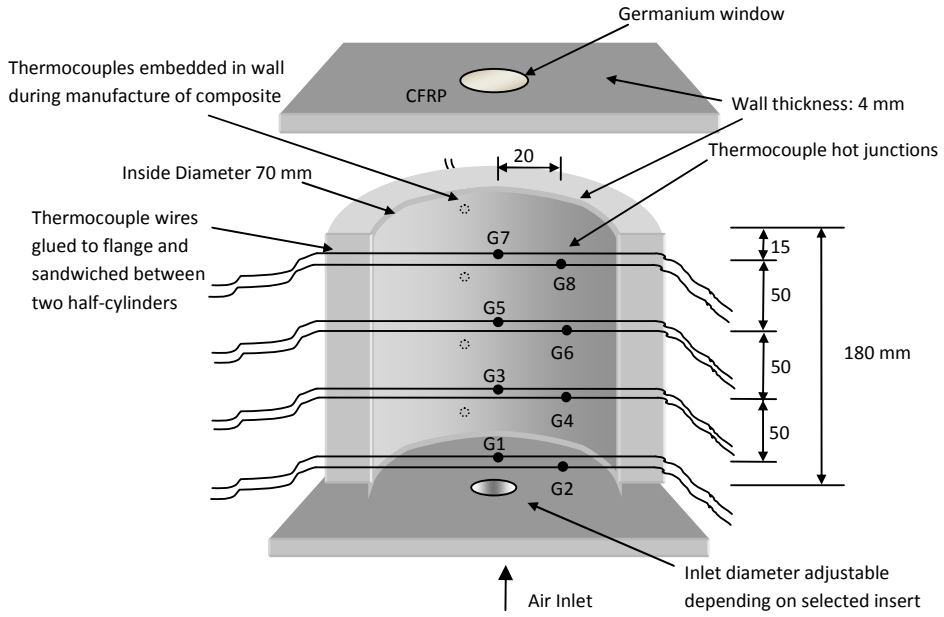

Fig. 1 CFRP vessel construction, geometry and thermocouple positions

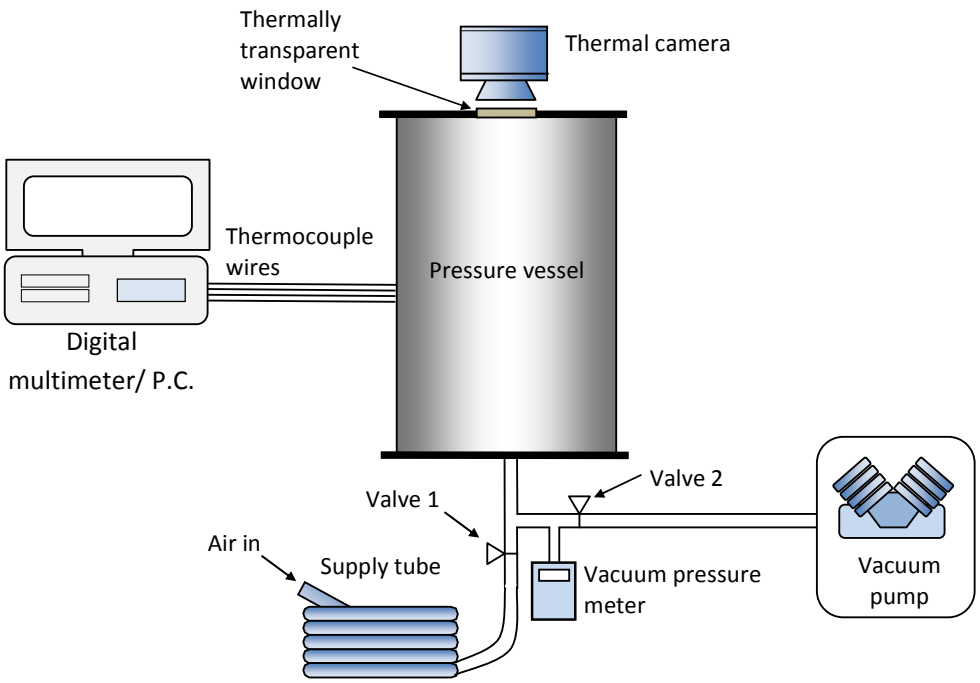

Fig. 2 Experimental setup

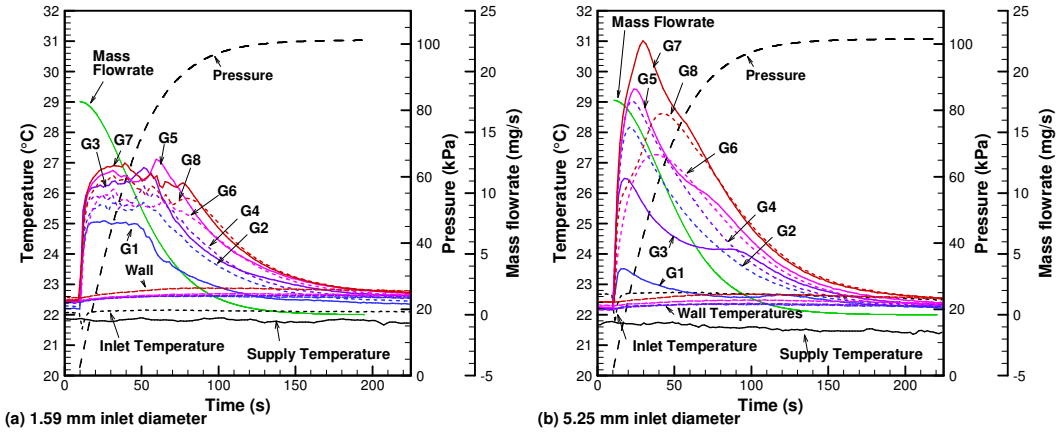

Fig. 3 Measured temperatures during filling of the vessel. The locations of the thermocouples are illustrated in Fig. 1

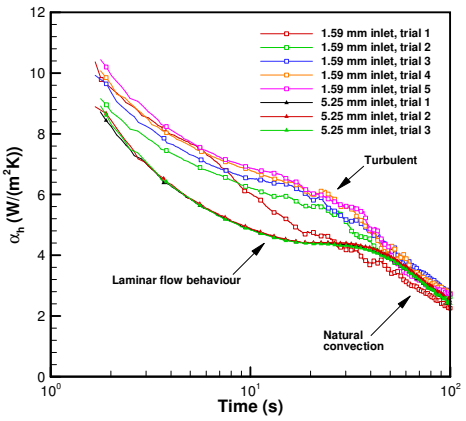

Fig. 4 Measured heat transfer coefficients during filling the vessel.

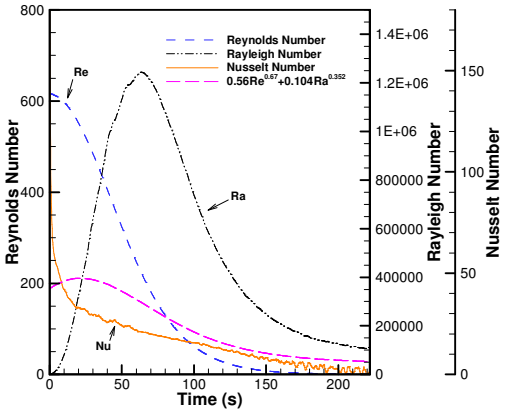

Fig. 5 Measured dimensionless groups

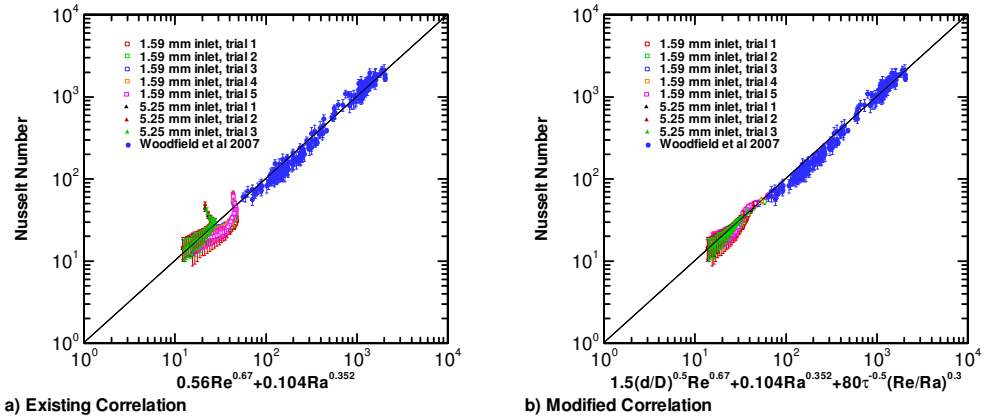

Fig. 6 Comparison of measured Nusselt number with correlations